frontiers | Frontiers in Earth Science

TYPE Original Research
PUBLISHED 07 March 2025
DOI 10.3389/feart.2025.1515701

OPEN ACCESS

EDITED BY
Peng Wu,
Dalian University of Technology, China

REVIEWED BY
Muhsan Ehsan,
Bahria University, Pakistan
Zhengzheng Cao,
Henan Polytechnic University, China

*CORRESPONDENCE
Xuefeng Yang,
yangxf-dq@petrochina.com.cn
Zimeng Xing,
xzm0777777@163.com

RECEIVED 23 October 2024
ACCEPTED 06 February 2025
PUBLISHED 07 March 2025

CITATION
Zhao H, Yin S, Yang X, Yan W, Bi G, Zhang J and Xing Z (2025) The influence of heterogeneity of lacustrine shale facies on rock mechanical properties and brittleness: a case study of Jurassic lacustrine shale reservoirs in Northeast Sichuan Basin. *Front. Earth Sci.* 13:1515701. doi: 10.3389/feart.2025.1515701

The influence of heterogeneity of lacustrine shale facies on rock mechanical properties and brittleness: a case study of Jurassic lacustrine shale reservoirs in Northeast Sichuan Basin

Haibo Zhao[1,2], Shujun Yin[1,2], Xuefeng Yang[1,2]*, Weilin Yan[1,2], Guangwu Bi[1,2], Jianliang Zhang[1,2] and Zimeng Xing[3]*

[1]State Key Laboratory of Continental Shale Oil, Daqing, China, [2]Exploration and Development Research Institute of PetroChina Daqing Oilfield Co., Ltd., Daqing, China, [3]College of Energy (College of Modern Shale Gas Industry), Chengdu University of Technology, Chengdu, China

Introduction: Due to the significant increase in plasticity under conditions of high temperature and pressure, the existing single brittleness evaluation methods prove inadequate for accurately characterizing the compressibility of deep shale in northeastern Sichuan, thereby severely limiting the optimal target selection and engineering modification in this region.

Methods: The focus of this paper is the deep Jurassic shale in northeastern Sichuan, studied through triaxial high-temperature and high-pressure tests, tensile tests, and X-ray diffraction experiments, which examine the mechanical properties of shale and the factors influencing them. The morphological characteristics of rock fractures under various loading conditions are analyzed, providing a standard for assessing brittleness factors and conducting a comprehensive quantitative evaluation.

Results: The research concludes that the deep lacustrine shale exhibits traits of high elastic modulus and high Poisson's ratio, with its brittleness largely influenced by mineral composition, the development characteristics of lamination, the degree of lamination development, and the anisotropy of the rock. Crack patterns have been analyzed to investigate the morphology of rock fractures. Through a correlation analysis of normalized rock parameters and the brittleness index derived from stress-strain curves with the fracture breakdown pressure and extension pressure observed in field fracturing, a comprehensive evaluation index has been established using the analytic hierarchy process to reflect the brittleness of deep lacustrine shale.

Discussion: This index serves effectively in characterizing the brittleness features of deep lacustrine shale, and evaluations suggest that the Liang upper section

has a relatively high brittleness index and good compressibility, marking it as a key target layer for future shale gas development.

KEYWORDS

deep shale, brittleness assessment, tensile testing, rock mechanics, factors influencing

1 Introduction

Over the last two decades, rapid development has been observed in China′s shale oil and gas industry, which has propelled the shale revolution, resulting in notable improvements in industrial output and theoretical research (Jin et al., 2021; Lei and Zhijun, 2019; Xuefeng et al., 2024).China′s shale oil output was 3.4 million tons in 2022, with an expected production of over 4.2 million tons in 2023, indicating significant development potential for shale oil in the country. In 2022, the production of shale oil in China was 3.4 million tons, and production is expected to surpass 4.2 million tons in 2023, indicating a substantial potential for development in the shale oil sector (Du et al., 2009; Guo et al., 2022). In 2024, the Xingye nine well drilled by Sinopec in the second section of the Lianggaoshan formation in the Fuxing area achieved horizontal well test results of 108.15 m^3 of oil and 15,800 m^3 of gas per day, representing a major breakthrough in shale oil exploration within the Sichuan Basin, as well as validating the significant exploration potential of shale oil in northeastern Sichuan (He et al., 2022). Nonetheless, the existing technological processes for shale oil exploration and development are not sufficiently comprehensive. The terrestrial shale reservoirs of the Jurassic Lianggaoshan formation have a high clay mineral content, complex structures, and relatively strong plasticity, leading to significant challenges in hydraulic fracturing. The mechanical properties of shale represent an essential element in the evaluation of shale gas reservoirs, and hydraulic fracturing is recognized as the fundamental technology for shale gas development. A precise comprehension of shale′s mechanical properties can offer valuable references for its hydraulic fracturing.

The mechanical properties of rock refer to its brittleness, plasticity, rheology, toughness, and other mechanical characteristics exhibited under stress. For shale reservoirs, the brittleness of the shale reservoir significantly impacts the effectiveness of shale gas extraction. Shale with higher brittleness favors the development of natural fractures. When effective fracturing measures are employed, it is easier to form complex network fractures with flow conductivity, thereby enabling efficient shale gas development (Jiang et al., 2010; Fu et al., 2011; Qinghui et al., 2012a; Zhang et al., 2017). Consequently, an increasing number of domestic and international scholars have begun to focus on evaluating the mechanical properties and brittleness of shale reservoir rocks (Jarvie et al., 2007; Zhang et al., 2016; Zhong et al., 2018). Cai Meifeng et al. argue that the brittleness and plasticity of rock are not inherent properties but can transform into each other as the stress state changes (Zhang et al., 2018; Cai et al., 2002; Cao et al., 2024c). Rickman and Altindag consider brittleness an intrinsic property of rock and suggest that external mechanical conditions, fractures, and other factors should not be considered when assessing it (Zheng, 1988; Rickman et al., 2008; Xiong et al., 2024; Sang et al., 2023; Cao et al., 2024a). Li Qinghui et al. propose that brittleness is the ability to generate internal non-uniform stress under its own heterogeneity and loading, leading to localized failure and the formation of multi-dimensional fracture surfaces (Altindag, 2010; Qinghui et al., 2012b; Qinghui et al., 2012c; Juyuan, 2013). Zhang et al. (2017) found that establishing evaluation indicators for rock brittleness can effectively reflect its mechanical characteristics of brittle fracture, making it the most intuitive and effective method for macroscopic brittleness evaluation at present. However, this method is limited by the relatively low efficiency and high cost of the experiments themselves. Regarding the brittle mineral composition method, Jarvie et al. (2007) initially believed that quartz was the only brittle mineral. However, as research has progressed, more scholars now recognize that feldspar, dolomite, and calcite also contribute to rock brittleness (Cao et al., 2024b; Cao et al., 2024c; Ehsan et al., 2024a; Cao Feng et al., 2024; Ehsan et al., 2024b; Amjad et al., 2023; Ziba et al., 2023; Saberi and Hosseini-Barzi, 2024).However, there is currently a lack of research on the impact of lithofacies heterogeneity in lacustrine shale reservoirs on rock mechanics and brittleness. There is an urgent need to establish interpretation methods and models applicable to the evaluation of rock mechanics, brittleness, and fracturability of various lithologies in the Jurassic system.

This paper will draw upon the results of various rock mechanics experimental tests, including triaxial high-temperature and high-pressure mechanical experiments, tensile strength experiments, and X-ray diffraction experiments. The innovative aspect lies in deeply revealing the specific factors influencing the rock mechanics properties and brittleness of lacustrine shale reservoirs due to petrographic heterogeneity, providing a new perspective for understanding the complex nature of shale reservoirs. Based on the analysis of morphological characteristics and mechanical properties of rock fracture cracks, a comprehensive index is innovatively constructed to quantitatively characterize the brittleness of terrestrial shale reservoirs with complex structures. The aforementioned research findings provide significant technical support for the selection of vertically fractured intervals in deep shale gas reservoirs, contributing to the improvement of shale gas development efficiency.

2 Methods for sample preparation and experimentation

2.1 Sample preparation and experimental protocol

The samples for the experiments were sourced from the Jurassic lacustrine shale in northeastern Sichuan. Because cores obtained from the field typically have irregular shapes, they require processing before being used in experiments. The sampling directions for the triaxial rock mechanics experiments were set to be longitudinal and transverse (Xuefeng et al., 2024; Biswas et al., 2024;

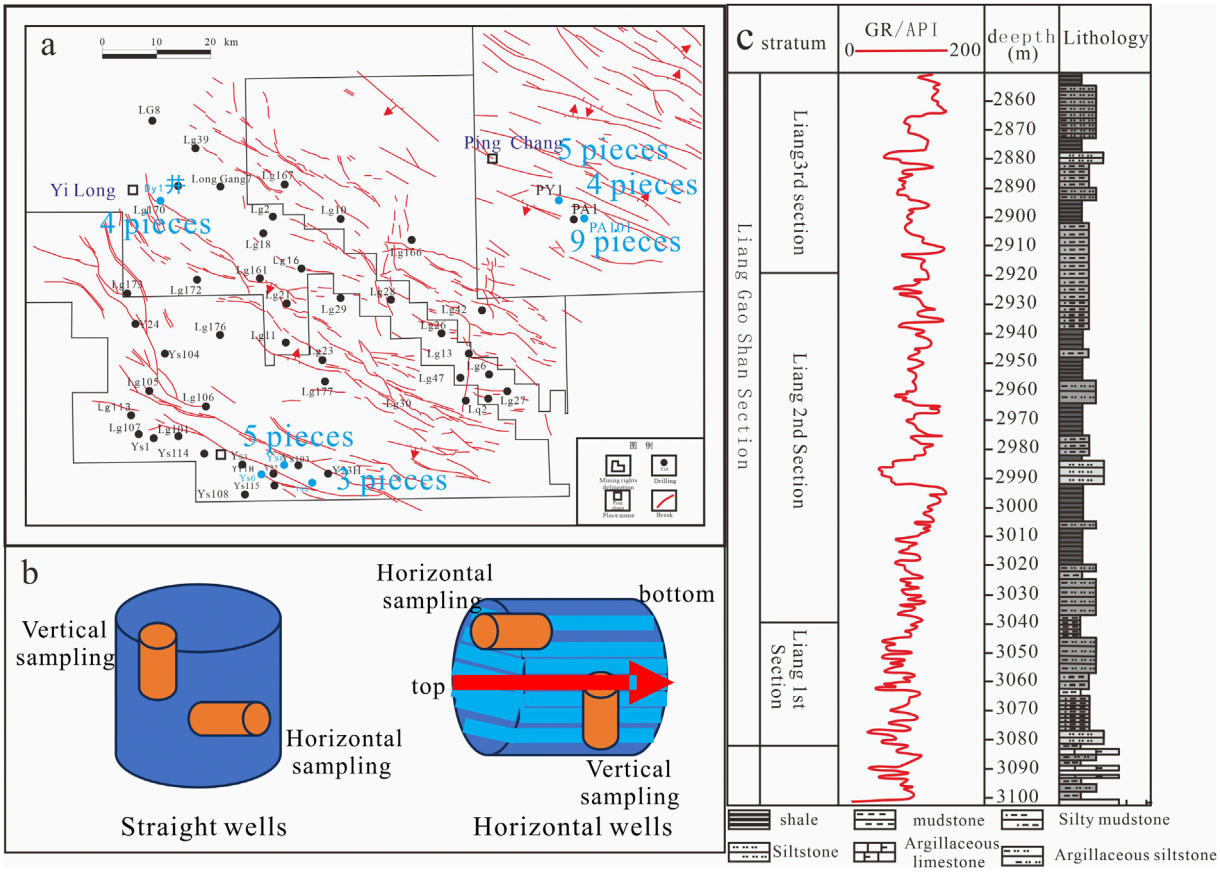

FIGURE 1
Schematic Diagram of Experimental Sampling. **(A)** Schematic Diagram of Sampling for Tri-axial High Temperature and High Pressure Experiment. **(B)** Schematic Diagram of Sampling for Tensile Test. **(C)** Histogram of the main lithologies in the area. Illustration of the experimental sampling process. (According to (Bai et al., 2024), after modification).

Banerjee et al., 2024) (Figure 1B). In the course of conducting high-temperature and high-pressure triaxial experiments, samples were consistently obtained in the transverse direction to investigate the influence of confining pressure and temperature on rock mechanical properties. Furthermore, control experiments for rock mechanics were established in both longitudinal and horizontal orientations, considering the actual temperature and pressure conditions of the reservoirs in the study area and averaging conditions based on prior

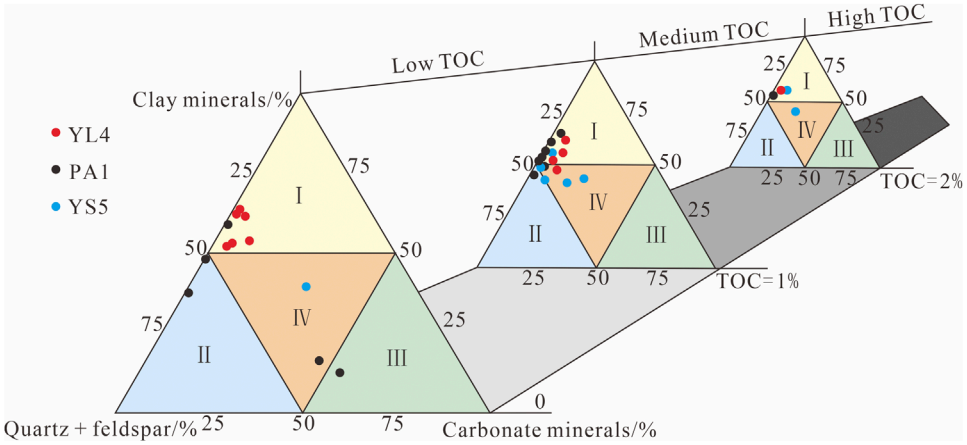

FIGURE 2
Diagram of mineral composition and lithofacies division of Lianggaoshan formation.

TABLE 1 Results of whole rock mineral diffraction in the Jurassic system.

Sample identification number	Well identification number	Depth (m)	Lithology	Quartz	K-feldspar	Plagioclase	Calcite	Dolomite	Baryte	Pyrite	Whewellite	Fluorapatite	Clay minerals
1	DY1	3180.32	Long-lived shale	48.0	—	21.5	0.6	—	0.9	—	—	—	29.0
2	DY1	3365.37	Clay-rich shale	43.4	—	8.2	8.7	—	—	6.2	—	—	33.5
3	DY1	3375.35	Mixed shale	27.3	—	1.9	22.4	—	—	2.4	—	—	46.0
4	DY1	3490.8	Calcareous shale	26.9	0.6	3.1	18.5	—	—	1.0	—	—	49.9
5	PY1-2H	3449.15	Fine sandstone	50.6	—	28.1	1.2	—	—	—	—	—	20.1
6	PY1-2H	3459.12	Stratified fine sandstone	50.6	—	29.9	5.1	—	—	—	—	—	14.4
7	PY1-2H	3550.41	Stratified fine sandstone	35.5	—	27.0	21.6	—	—	—	—	—	15.9
8	PY1-2H	3462.41	Stratified fine sandstone	48.0	—	28.3	5.2	—	—	—	—	—	18.5
9	PA101	3160	Laminated clay-rich shale	46.3	—	19.7	11.9	—	0.9	0.8	—	3.0	17.4
10	PA101	3160.8	Clay-rich shale	39.9	—	19.3	16.1	—	—	0.7	—	—	24.0
11	PA101	3333.55	Fine sandstone	47.4	—	17.4	0.8	—	—	—	—	—	34.4
12	PA101	3335.58	Fine sandstone	43.8	—	17.5	—	—	—	—	—	—	38.7
13	PA101	3340.58	Fine sandstone	48.3	—	22.8	—	—	—	—	—	—	28.9
14	PA101	3359.62	Long-lived shale	37.2	—	12.5	—	—	—	—	—	—	50.3

(Continued on the following page)

10.3389/feart.2025.1515701

TABLE 1 (*Continued*) Results of whole rock mineral diffraction in the Jurassic system.

Sample identification number	Well identification number	Depth (m)	Lithology	Quartz	K-feldspar	Plagioclase	Calcite	Dolomite	Baryte	Pyrite	Whewellite	Fluorapatite	Clay minerals
15	PA101	3159	Laminated clay-rich shale	30.3	—	2.3	19.8	1	—	3.1	—	—	43.5
16	PA101	3166.38	Clay-rich shale	28.9	—	2	21.9	2.2	—	3.6	—	—	41.4
17	PY1-5H	3553.2	Laminated clay-rich shale	32.9	—	4.5	3.9	0	—	0.6	—	—	58.1
18	PY1-5H	3561.06	Clay-rich shale	28.9	—	2.4	19.5	1.3	—	3.6	—	—	44.3
19	PY1-5H	3554.3	Laminated clay-rich shale	37.8	—	7.7	—	—	—	—	—	—	54.5
20	PY1-5H	3562.82	Mixed shale	31.6	—	8.5	12.1	—	—	—	—	—	47.8
21	PY1-5H	3563.82	Calcareous shale	35.6	—	7.0	—	—	—	—	—	—	57.4
22	YS5	1893.9	Clay-rich shale	33.9	—	5.0	7.1	—	—	1.4	—	—	52.6
23	YS5	1895.5	Calcareous shale	32.3	—	1.9	9.6	—	—	2.9	—	—	53.3
24	YS8	1699.78	Calcareous shale	10.5	—	—	76.3	—	—	1.5	3.6	—	8.1
25	YS8	1823.75	Mixed shale	19.4	0.7	2.0	28.7	—	—	1.3	—	4.0	43.9
26	YS8	1812.79	Laminated mixed shale	28.8	—	3.1	18.2	2.1	—	2.7	—	—	45.1
27	YS8	1816.9	Clay-rich shale	19.9	—	0.7	43.5	10.1	—	2.3	—	—	23.5
28	YS8	1819.66	Laminated mixed shal	26.9	—	2.2	31	0.9	—	2.1	—	—	36.9

(Continued on the following page)

10.3389/feart.2025.1515701

10.3389/feart.2025.1515701

TABLE 1 (*Continued*) Results of whole rock mineral diffraction in the Jurassic system.

Sample identification number	Well identification number	Depth (m)	Lithology	Quartz	K-feldspar	Plagioclase	Calcite	Dolomite	Baryte	Pyrite	Whewellite	Fluorapatite	Clay minerals
29	YS8	1824.78	Clay-rich shale	26.2	—	5.1	2.2	—	—	2	—	—	64.5
30	YS8	1832.87	Clay-rich shale	36.6	—	5	0.8	—	—	—	—	—	57.6
31	YS8	1835.03	Clay-rich shale	33.3	—	4.6	—	—	—	—	—	—	62.1
32	YS8	1839.17	Shell limestone	33.4	—	7.6	18	—	—	1.2	—	—	39.8

experiments. The experimental conditions for the rock mechanics tests were established as follows: Ying Mountain block (YS5 and YS8 wells): 20 MPa and 50°C; Pingchang block (PY1-2H, PY1-5H, and PA101 wells): 30 MPa and 70°C; Longgang block (DY1 well): 30 MPa and 70°C. The sampling directions for tensile experiments were set to be vertical and horizontal. Taking into account the coverage of the samples, differences in reservoir conditions, vertical segment distribution, and core collection status, along with the distribution of lithofacies, sedimentary structures, and fractures in the study area, 260 samples from nine different categories across six wells—PY1-2H, PY1-5H, PA101, DY1, YS5, and YS8—were collected and processed (Figure 1A). Figure1C is a histogram of the main lithologies in the area.

2.2 Experimental methods

The mechanical parameters of rock cores are determined using a high-temperature and high-pressure triaxial testing apparatus, specifically the RTR-1000 Static (Dynamic) Triaxial Rock Mechanics Testing System from GCTS Corporation in the United States. This comprehensive setup consists of four main components: a high-temperature and high-pressure triaxial chamber, a confining pressure system, an axial pressure system, and an automatic data acquisition and control system. The apparatus complies with ASTM D2664-04 standards and the recommended methods for rock mechanics experiments by the International Society for Rock Mechanics and Rock Engineering (Qinghui et al., 2012a; Jarvie et al., 2007; Reedy et al., 2024). The testing system boasts a maximum axial load of 1,000 kN, a maximum confining pressure of 140 MPa, a pore pressure of 140 MPa, a dynamic frequency of 10 Hz, and a temperature of 150°C. The experimental control precision is as follows: pressure: 0.01 MPa; liquid density: 0.01 g/cm^3; deformation: 0.001 mm. The testing is conducted at an ambient temperature ranging from 200°C to 230°C and a humidity of 64% RH, utilizing a lateral isobaric triaxial testing method (Li et al., 2024; Chakladar et al., 2024).

During the tensile strength testing, a 50 KN electronic servo system is employed to conduct a splitting test on standard specimens until the rock reaches its tensile limit and fractures. Corresponding parameters are then calculated. The testing procedures are strictly implemented according to the DZ/T 0276.21-2015 "Rock Tensile Strength Testing" standard. The experimental control precision for this test is: pressure of 0.05 MPa and deformation of 0.001 mm (Li et al., 2024).

For whole-rock XRD mineral analysis, a DX-2700 X-ray diffractometer is used to determine the mineral composition and clay content of reservoir rocks. Powder samples are thoroughly crushed using a sample crusher to a size of approximately 5 mm. Based on the diffraction data obtained from the testing, including diffraction curves, d-values, relative intensities, and diffraction peak widths, analysis software is utilized on a computer to conduct whole-rock and clay mineral composition analysis (Cao Feng et al., 2024).

The porosity of rocks (helium method) is calculated using a PHI-220 automatic porosity tester. This method exploits the principle that the diffusion rate of helium in pores is directly proportional to porosity. By measuring the diffusion rate of helium in shale, porosity can be calculated. The porosity and permeability

TABLE 2 Results of high-temperature and high-pressure triaxial rock mechanics experiment in shale reservoir.

Experimental sample number	Well Identifier	Depth (m)	Lithology	Containment (MPa)	Temperature (°C)	Sampling direction	Poisson's ratio	Young's modulus (MPa)	Compressive strength (MPa)
1	YS5	1893.9–1894.03	Clayey shale	20	50	Horizontal	0.150	14,147.9	59.9
2	YS5	1895.5–1895.72	Gray shale	20	50	Vertical	0.169	6342.6	51.6
3	YS8	1699.78–1699.93	Gray shale	20	50	Vertical	0.174	8373.6	55.4
4	YS8	1823.75–1823.9	Mixed shale	20	50	Vertical	0.180	5862.5	62.7
5	YS8	1812.79–1812.87	Stratiform mixed shale	20	50	Horizontal	0.167	27,302.4	106.4
6	YS8	1816.90–1816.97	Clayey shale	20	50	Vertical	0.192	9779.6	68.4
7	YS8	1819.66–1819.74	Stratiform mixed shale	20	50	Horizontal	0.275	31,147.2	102.3
8	YS8	1824.78–1824.86	Clayey shale	20	50	Vertical	0.178	6509.7	56.2
9	YS8	1832.87–1832.95	Clayey shale	20	50	Horizontal	0.214	34,822.1	74.8
10	YS8	1835.03–1835.10	Clayey shale	20	50	Horizontal	0.206	34,827.7	67.2
11	YS8	1839.17–1839.25	Mesoshell limestone	20	50	Vertical	0.155	50,458.3	232.5
12	DY1	3180.32–3180.56	Felsic shale	30	70	Horizontal	0.209	27,982.5	179.0
13	DY1	3365.37–3365.55	Mixed shale	30	70	Vertical	0.208	7124.9	92.3
14	DY1	3375.35–3375.55	Clayey shale	30	70	Horizontal	0.236	13,531.7	73.7
15	DY1	3490.8–3491.06	Gray shale	30	70	Vertical	0.156	11,610.3	79.4
16	PA101	3160–3160.12	Stranded clayey shale	30	70	Vertical	0.249	29,773.2	108.8
17	PA101	3160.8–3161	Clayey shale	30	70	Horizontal	0.239	27,139.2	141.9
18	PA101	3333.55–3333.64	Fine sandstone	30	70	Vertical	0.215	29,181.7	135.6
19	PA101	3335.58–3335.67	Fine sandstone	30	70	Vertical	0.202	22,978.7	121.6
20	PA101	3340.58–3340.67	Fine sandstone	30	70	Horizontal	0.248	23,894.8	141.9

(Continued on the following page)

10.3389/feart.2025.1515701

TABLE 2 (*Continued*) Results of high-temperature and high-pressure triaxial rock mechanics experiment in shale reservoir.

Experimental sample number	Well Identifier	Depth (m)	Lithology	Containment (MPa)	Temperature (°C)	Sampling direction	Poisson′s ratio	Young′s modulus (MPa)	Compressive strength (MPa)
21	PA101	3340.58–3340.67	Fine sandstone	30	70	Vertical	0.152	27,449.8	136.1
22	PA101	3359.62–3359.71	Felsic shale	30	70	Horizontal	0.367	11,152.0	55.3
23	PY1-5H	3160–3160.12	Stranded clayey shale	30	70	Horizontal	0.243	19,085.7	101.6
24	PY1-5H	3554.3–3554.62	Mixed shale	30	70	Horizontal	0.166	25,185.0	130.4
25	PY1-5H	3562.82–3563.22	Gray shale	30	70	Vertical	0.153	12,015.1	69.5
26	PY1-2H	3563.82–3564.12	Fine sandstone	30	70	Horizontal	0.167	31,643.8	227.7
27	PY1-2H	3449.15–3449.5	Fine sandstone	30	70	Vertical	0.130	31,112.2	233.8
28	PY1-2H	3449.15–3449.5	Bedding fine sandstone	30	70	Horizontal	0.205	34,894.4	267.6
29	PY1-2H	3459.12–3459.48	Bedding fine sandstone	30	70	Horizontal	0.221	33,538.4	223.3
30	PY1-2H	3550.41–3550.78	Bedding fine sandstone	30	70	Vertical	0.265	29,553.9	217.2
31	PY1-2H	3550.41–3550.78	Bedding fine sandstone	30	70	Horizontal	0.197	32,773.6	232.2
32	PY1-2H	3462.41–3462.7	Bedding fine sandstone	30	70	Vertical	0.199	32,969.4	194.7

10.3389/feart.2025.1515701

TABLE 3 Classifications of triaxial stress-strain curves of shale under high pressure and high temperature.

Type	Image	Feature points	Lithology
Type 1: The pre-peak behavior is defined by elastic-plastic characteristics. Post-peak, the material displays significant brittleness, with strain hardening noted during the decline in strength.	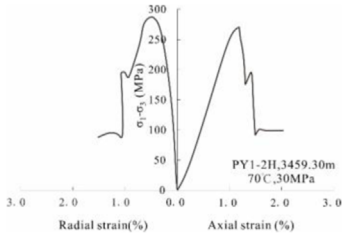	Yield-to-peak ratio: 0.833 Weakening modulus: -9620.871	Fine sandstone Bedding fine sandstone Felsic shale
Type 2: The pre-peak behavior is defined by a largely elastic-plastic response. A considerable amount of plasticity is evident in this category, resulting in pronounced brittleness following the peak.	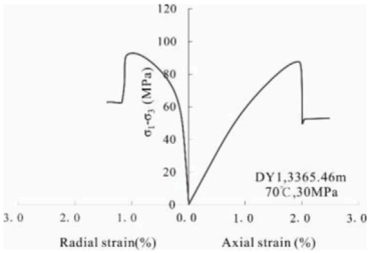	Yield-to-peak ratio: 0.647Modulus of weakening: -10224.7	Clayey shale Stratiform mixed shale Gray shale
Type 3: The pre-peak behavior is defined by elastic characteristics. Moderate brittleness occurs post-peak, reflecting a transitional behavior.	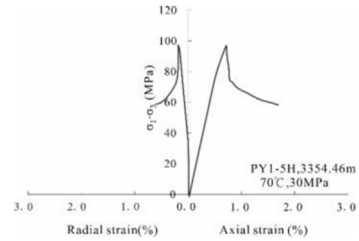	Yield-Peak Ratio: 0.855 Deterioration Modulus: -512.87	Stratified Clay-rich Shale Mesoshell limestone Felsic shale
Type 4: The pre-peak behavior is defined by elastic characteristics. Following the peak, the material demonstrates plastic behavior.	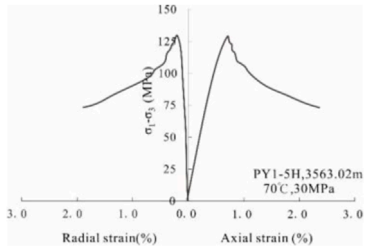	Yield-Peak Ratio: 0.92 Deterioration Modulus: -141.277	Mixed shale Clayey shale
Type 5: The pre-peak behavior is defined by a combination of elastic and plastic characteristics. After reaching the peak, the material retains its plastic behavior.	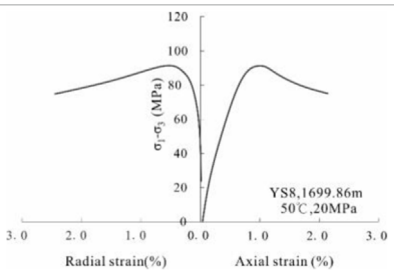	Yield-Peak Ratio: 0.59 Deterioration Modulus: -79.068	Gray shale

of the samples are analyzed using the GB-T 29172-2012 core analysis method (Xuefeng et al., 2024).

3 Results

3.1 Study on petrology and lithofacies characteristics

The mineral composition of shale is primarily comprised of clastic components (such as quartz and felspar), matrix materials (like clay minerals), and cementing materials (such as carbonate minerals). The traditional classification divides it into four major categories based on the content of quartz-feldspar, clay minerals, and carbonate minerals: I, Clayey Shale (CAS); II, Silty Shale (SYS); III, Calcareous Shale (CS); IV, Mixed Shale (BS).IV. Mixed shale (BS). This classification is based on the mineral content characteristics of the study area and the influence of organic carbon in shale oil reservoirs, with 1% and 2% designated as the thresholds for total organic carbon (TOC) content. Three categories are identified: low, medium, and high organic carbon (Ehsan et al., 2024a; Amjad et al., 2023) (Figure 2). Furthermore, four lithofacies are classified: I. Long-feldspar shale facies (feldspar + quartz > 50%); II. Calcareous shale facies (carbonate minerals > 50%); III. Clay-rich shale facies (clay minerals > 50%); IV. Mixed shale facies

TABLE 4 Results of high-temperature and high-pressure triaxial rock mechanics experiment in shale reservoir.

Experimental sample number	Well Identifier	Depth (m)	Lithology	Sampling direction	Length (mm)	Diameter (mm)	Maximum load (KN)	Tensile strength (MPa)
1	YS5	3554.46	Layered Clayey Shale	Vertical	24.80	25.10	10.414	10.65
2	YS5	3563.02	Mixed Shale	Horizontal	24.66	25.16	3.815	3.91
3	YS8	3563.97	Grey Shale	Vertical	25.56	25.06	7.172	7.13
4	YS8	3449.325	Fine Sandstone	Horizontal	23.62	25.25	16.518	17.63
5	YS8	3449.325	Fine Sandstone	Vertical	24.56	25.27	14.687	15.07
6	YS8	3459.3	Layered Fine Sandstone	Vertical	25.08	25.33	13.276	13.30
7	YS8	3550.595	Layered Fine Sandstone	Horizontal	25.19	25.10	12.741	12.83
8	YS8	3550.595	Layered Fine Sandstone	Vertical	24.86	25.15	13.657	13.91
9	YS8	3462.555	Layered Fine Sandstone	Horizontal	24.62	25.14	15.831	16.28
10	YS8	3462.555	Layered Fine Sandstone	Vertical	24.70	25.19	11.330	11.59
11	YS8	3160	Layered Clayey Shale	Vertical	15.30	25.08	7.515	12.47
12	DY1	3160.8	Clayey Shale	Horizontal	19.97	25.33	9.728	12.24
13	DY1	3333.55	Fine Sandstone	Vertical	25.26	25.04	9.651	9.71
14	DY1	3335.58	Fine Sandstone	Vertical	25.04	25.08	5.036	5.11
15	DY1	3340.58	Fine Sandstone	Horizontal	24.02	25.08	18.082	19.11
16	PA101	3340.58	Fine Sandstone	Vertical	24.48	25.10	11.711	12.13
17	PA101	3359.62	Felsic shale	Horizontal	25.14	25.07	4.349	4.39
18	PA101	3180.44	Felsic shale	Vertical	24.93	25.21	14.229	14.41
19	PA101	3365.46	Clayey Shale	Horizontal	25.22	24.68	2.060	2.11
20	PA101	3375.45	Heterogeneous Shale	Vertical	24.85	24.92	5.303	5.45
21	PA101	3490.93	Grey Shale	Vertical	25.53	25.18	4.234	4.19
22	PA101	1893.965	Clayey Shale	Horizontal	25.12	25.02	5.264	5.33

(Continued on the following page)

10.3389/feart.2025.1515701

TABLE 4 (*Continued*) Results of high-temperature and high-pressure triaxial rock mechanics experiment in shale reservoir.

Experimental sample number	Well Identifier	Depth (m)	Lithology	Sampling direction	Length (mm)	Diameter (mm)	Maximum load (KN)	Tensile strength (MPa)
23	PY1-5H	1895.61	Grey Shale	Vertical	25.50	25.06	7.668	7.64
24	PY1-5H	1699.855	Grey Shale	Horizontal	21.26	24.96	2.441	2.93
25	PY1-5H	1823.825	Heterogeneous Shale	Vertical	24.91	25.08	9.156	9.33
26	PY1-2H	1812.87	Layered Mixed Shale	Horizontal	25.14	25.16	1.099	1.11
27	PY1-2H	1816.97	Clayey Shale	Horizontal	24.97	25.09	3.711	3.77
28	PY1-2H	1819.74	Layered Mixed Shale	Horizontal	25.04	25.23	4.519	4.55
29	PY1-2H	1824.86	Clayey Shale	Horizontal	25.01	25.18	5.962	6.03
30	PY1-2H	1932.95	Clayey Shale	Horizontal	24.99	24.92	5.039	5.15
31	PY1-2H	1835.10	Clayey Shale	Horizontal	25.27	25.25	1.426	1.42
32	PY1-2H	1839.25	Shell limestone	Horizontal	25.03	25.15	3.830	3.87

10.3389/feart.2025.1515701

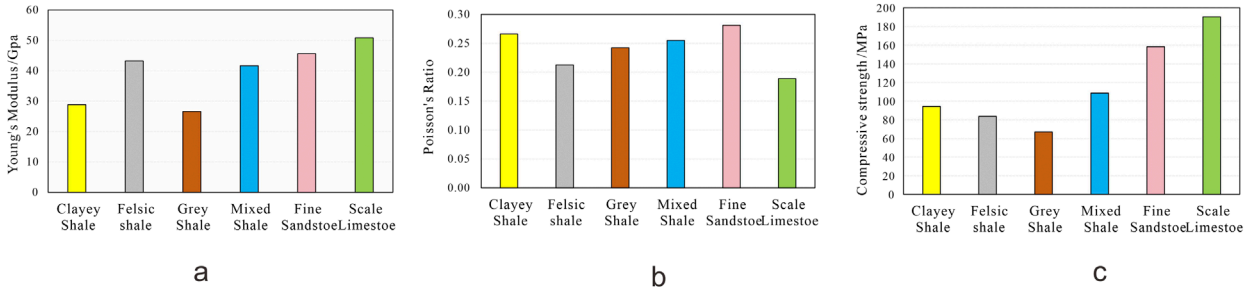

FIGURE 3
Distribution Diagram of Rock Mechanics Parameters for Different Homogeneous Lithologies in Tri-axial Experiments. **(A)** Transverse elastic modulus of homogeneous rock; **(B)** Transverse Poisson′s ratio of homogeneous rock. **(C)** Transverse compressive strength of homogeneous rock.

(no mineral component exceeds 50%). The lithology analyzed displays considerable diversity, particularly with higher amounts of clay minerals (Ehsan et al., 2024b). The mineral composition of Jurassic shale is predominantly quartz and clay minerals, along with lesser amounts of plagioclase and calcite, and includes small quantities of pyrite. In the Liangshang section, plagioclase content is markedly higher compared to the Danzhai and Dongyuemiao sections, suggesting a more substantial impact from proximate sediment sources. In general, the mineral compositions vary greatly among different lithologies. Sandstones are mainly characterized by high contents of quartz and feldspar, whereas shales show substantial variations, predominantly composed of quartz and clay minerals. Notably, the calcareous shale in the Danzhai section has a higher concentration of calcite. Within the study area, the rocks predominantly display three categories of lamination structures: organic-rich lamination, sand-rich lamination, and calcareous lamination (Table 1).

3.2 Results of triaxial compression rock mechanics experiments

Results from the tests of rock mechanics parameters under triaxial loading conditions are shown in Tables 2, 3 presents the stress-strain curves of selected rock samples, indicating that shale samples transition from elastic deformation to fracturing under low-temperature pressure, whereas at high-temperature pressure, the peak stress is reached more slowly, and significant residual stress is maintained after rupture. As the confining pressure increases, the pores and microfractures within the rock are generally subjected to intense compression from the surrounding rock. The stress-strain curves are categorized into five types based on the morphology and characteristic points of the three stages of the stress-strain relationship. The first three types indicate strong brittleness in the rocks, mainly represented by sandstone, leucogranite shale, and laminated clay shale, with notable differences in mechanical properties observed in both horizontal and vertical orientations (Table 3). The complexity of the fracture patterns in rock samples is a fundamental indication of brittleness. This study primarily identified single shear failure as the fracture mode, with samples largely remaining intact after fracturing. As the uniformity of the rock increases, the elastic properties become stronger, resulting in more complex fractures. Furthermore, if the rock contains layered structures, the fracture mode varies with the orientation of these layers. Supplementary Explanation S1 illustrates that at a pressure of 20 MPa, the fracture characteristics of the rock samples are predominantly of the splitting type, with shear fractures being secondary. Cracks mainly develop axially, showing complex morphologies, with notable fragmentation of the samples. Under the condition of 30MPa, the crack extends to another group of cracks and terminates, accompanied by microcracks at the end of longer cracks. Under this confining pressure, double shear type is dominant, and the fracture surface no longer follows the axis and presents a higher angle with the horizontal.The types of fractures in the rock can be classified into three categories: tensile failure occurs under conditions of high brittleness when axial stress surpasses compressive strength, resulting in tensile fractures along the axial direction, characterized by one or more sets of splitting cracks. Shear failure arises in rocks displaying strong plasticity, with large plastic deformations and evident lateral deformation leading to plastic shear failures. There is also a composite failure type, where the rock samples show both pronounced tensile splitting and shear fractures simultaneously. As the conditions transition from low temperature and low confinement pressure to high temperature and high confinement pressure, the fracture modes of the rock specimens change from a complex splitting-tensile type to a composite tensile-shear type, ultimately resulting in a pure shear type.

3.3 Tensile strength test results

Table 4 presents the partial results of rock mechanics parameter tests conducted under tensile strength loading conditions. The results of tensile strength tests for different lithologies in the Jurassic Formation this time vary significantly. Overall, the tensile strength of sandstones from the Lianggaoshan Formation is relatively high, generally exceeding 10 MPa. In contrast, the tensile strength of limestones and mudstones containing shells in the Da′anzai and Dongyuemiao sections is relatively low. Additionally, felsic shales and mixed shales have higher tensile strengths than clayey shales. The experiment revealed three primary fracture modes:

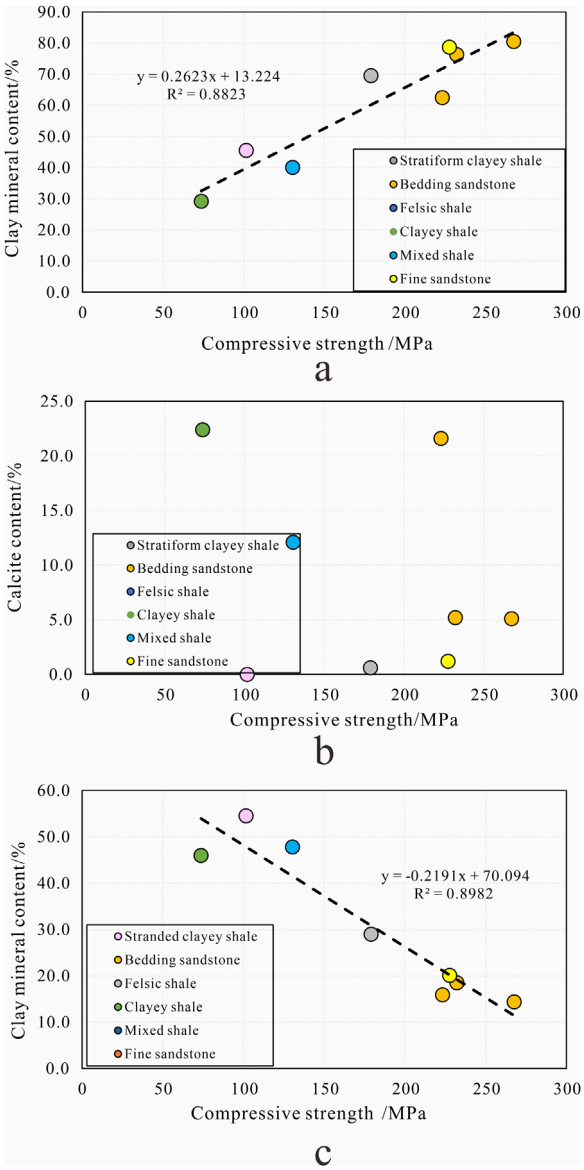

FIGURE 4
Diagram of the Relationship between Rock Mechanics Parameters and Mineral Composition for Different Homogeneous Lithologies in Tri-axial Experiments. **(A)** Correlation between Quartz + feldspar content minerals and compressive strength; **(B)** Correlation between calcite and compressive strength; **(C)** Correlation between clay minerals and compressive strength.

simple uniform longitudinal splitting, parallel longitudinal splitting, and intersecting shear and tensile fractures (Supplementary Explanation S2).

3.4 Analysis of influencing factors on rock mechanical propertie

3.4.1 Mineral composition and lithology

Under the same burial depth conditions, rock layers rich in brittle minerals are often more compressible than rock layers lacking brittle minerals (Qiao et al., 2020). The acquisition of mineral species and their composition ratios in strata is an important approach for identifying brittle and ductile layers (Rahimzadeh et al., 2018). Because lithological characteristics vary by region, the identification of brittle minerals must be integrated with specific analyses of sedimentary environments and lithology in different areas; nevertheless, quartz is always recognized as a brittle mineral (Jarvie et al., 2007; Zhang et al., 2016; Rickman et al., 2008; Nelson, 2001; Yuanyuan et al., 2021). Figure 3 illustrates the distribution of mechanical parameters for homogeneous lithological rocks under triaxial compression. The mechanical parameters vary among different homogeneous lithologies. The compressive strength and elastic modulus of sandstone and limestone exceed those of shale, with elastic moduli ranging from 25 to 50 MPa. Andesite shale and mixed shale exhibit greater strength compared to other lithologies, with their elastic moduli ranging from 22 to 34 MPa. In fine sandstone, simple through shear fractures are predominant, while clay-rich shales and chalky limestones exhibit both non-through shear fractures and splitting tensile veins (Supplementary Explanation S3). In general, compressive strength shows a positive correlation with andesite minerals and a negative correlation with clay minerals, with no clear relationship identified with calcite (Figure 4). Under tensile testing conditions, samples from various lithologies and strata demonstrate a characteristic where tensile strength is greater in the vertical direction than in the horizontal direction. The tensile strength difference of sandstone is notably smaller than that of mud shale. Generally, the tensile strength of sandstone surpasses that of shale and chalky limestone, with the latter exhibiting the lowest tensile strength due to its banded structure. The tensile strength of andesite shale is higher than that of mixed shale and calcareous shale (Figure 5). Higher quartz content correlates with greater tensile strength, while higher clay mineral content correlates with lower tensile strength (Figure 6). Following tensile strength experiments on homogeneous lithology samples, a predominant occurrence of simple uniform longitudinal splitting was observed (Supplementary Explanation S4).

3.4.2 Lamination development characteristics and degree of development

Bedding planes are identified as mechanical weak features within the rock, which affect fracture propagation paths during the fracturing process, including the redirection of induced fractures and the penetration and connection along bedding or between layers (Qiao et al., 2020; Zhao et al., 2019). Under triaxial loading conditions, the increase in argillaceous and quartz-rich bedding and brittle minerals leads to improved elasticity, a relative reduction in Poisson′s ratio, and a decrease in the compressive strength of the rock (Figure 7). The layered clay-rich and mixed shales predominantly display either shear or tensile fractures, while argillaceous gray shales reveal significant fracture propagation affected by quartzose and argillaceous bedding. Such rock types are characterized by a relatively high occurrence of shear fractures and shear slip propagation along the bedding planes. Conversely, layered sandstones show a greater prevalence of fractures extending along bedding, with fewer fractures penetrating through the bedding (Supplementary Explanation S5). Under uniform lithological conditions in tensile testing, the

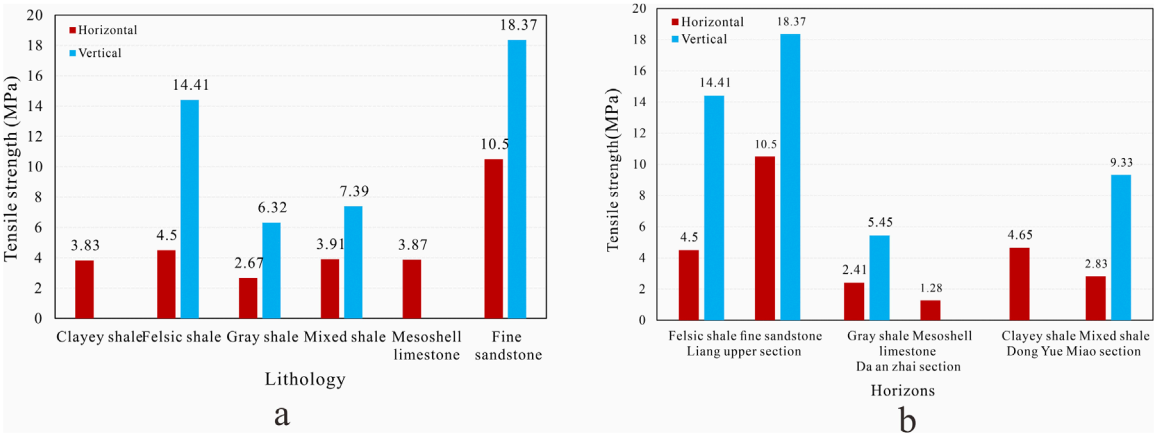

FIGURE 5
Comparison Chart of Tensile Strength Results for Homogeneous Lithologies in Tensile Tests. **(A)** Comparison of tensile strength results among various lithologies in homogeneous rock. **(B)** Comparison of tensile strength results for representative lithologies at various strata in homogeneous rock. Illustrates the comparison of tensile strength results obtained from tensile tests on homogeneous rock.

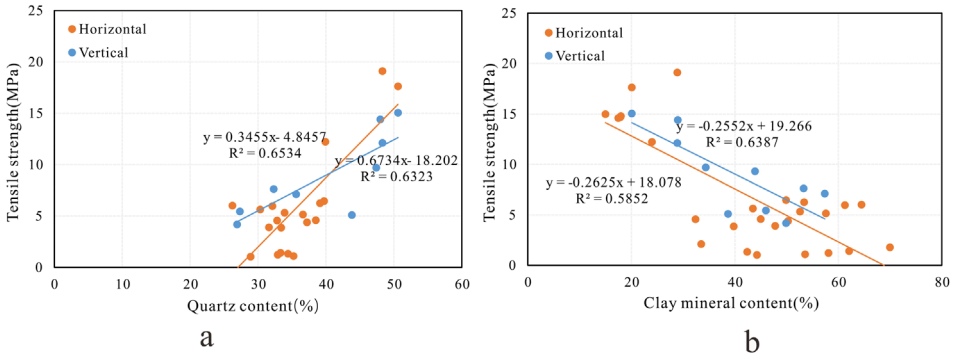

FIGURE 6
Diagram of the Relationship between Tensile Strength and Mineral Content in Tensile Tests. **(A)** Effect of quartz content on tensile strength in homogeneous rock. **(B)** Effect of clay mineral content on tensile strength in homogeneous rock.

tensile strength of laminated rocks shows a significant reduction, with longitudinal tensile strength found to be lower than transverse tensile strength (Figure 7). The fractures that occur parallel to the bedding are largely characterized by shear fractures, whereas the fractures that occur perpendicular to the bedding mainly consist of shear and tensile fractures (Supplementary Explanation S6), indicating some differences between sandstones and shales.

3.4.3 Rock anisotropy

Layering acts as a mechanical weak plane within the rock, affecting the propagation paths of fractures during the fracturing process, including induced fracture turning and the penetration and communication along or between the layers (Qiao et al., 2020; Yuan et al., 2021). In the presence of triaxial loading conditions, rock samples with developed layering show a more complex fracture network, with fractures primarily resulting from tensile-shear failure that penetrates the layers, leading to more convoluted crack shapes with small cracks at their ends. Conversely, rock samples with weaker layering display straight fractures that are simpler in shape than those in the former. In general, under the same experimental conditions and with uniform rock characteristics, the longitudinal elastic modulus and compressive strength exceed the transverse test values. Furthermore, the longitudinal Poisson′s ratio is lower than the transverse ratio, with the mechanical property differences becoming more pronounced after layering development (Figures 8A–C). Longitudinal samples predominantly show simple shear fractures after failure, whereas transverse samples exhibit not only similar shear fractures but also splitting cracks along the layering, with the influence of layered lithology being particularly evident. In tensile test conditions, transversely sampled rocks show more developed layering and a diminished ability to resist crack propagation. Consequently, in the tensile tests, the tensile strength of layered lithology is noticeably weakened compared to uniform rock properties, and the longitudinal tensile strength is less than the transverse tensile strength (Figure 8D). Fractures propagating along the layering direction are predominantly shear fractures, while the fracture patterns perpendicular to the layering

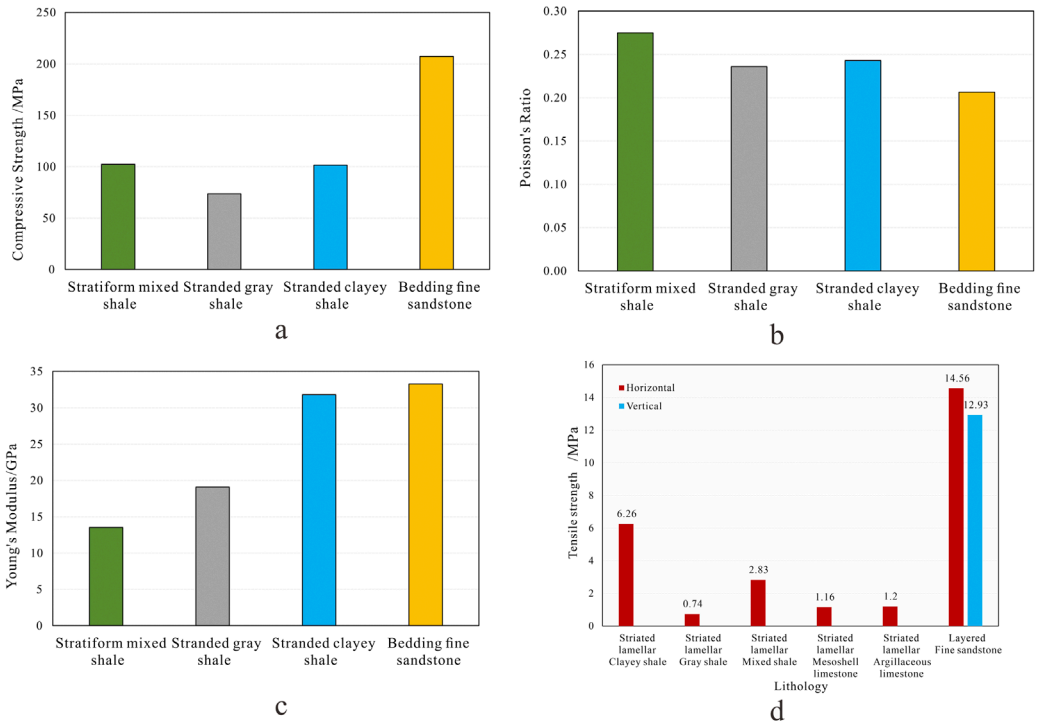

FIGURE 7
Effect of Laminations on Rock Mechanics Parameters. **(A)** Poisson′s ratio of layered specimens (horizontal). **(B)** Compressive strength of layered specimens (horizontal). **(C)** Elastic modulus of layered specimens (horizontal); **(D)** Comparison of tensile strength results for layered lithologies sampled in various orientations in tensile experiments.

direction are mainly characterized by shear and longitudinal tensile fractures; however, notable differences are present between sandstone and shale.

3.4.4 Temperature and surrounding pressure

In high-temperature and high-pressure triaxial testing conditions, confining pressure has a more substantial effect on the mechanical properties of shale and sandstone compared to temperature. As confining pressure increases, the elastic modulus and compressive strength show considerable increments, whereas the Poisson′s ratio experiences a slight increase. The mechanical characteristics of clayey shale demonstrate greater sensitivity to changes in confining pressure. With increasing temperature and confining pressure conditions, the rock samples evolve from composite shear fractures and splitting to single shear fractures, leading to a decrease in both the number and complexity of fractures (Figure 9).

4 Discussion

4.1 Brittleness index based on elastic parameters

R. Rickman et al. explored the brittleness index derived from elastic parameters, employing statistical regression methods. Their findings indicate that higher Young′s modulus and lower Poisson′s ratio correlate with enhanced brittleness. Additionally, they introduced a normalized calculation formula for brittleness based on Young′s modulus and Poisson′s ratio (Rickman et al., 2008) (Equations 1–3).

$$B_{brit} = 0.5E_{brit} + 0.5\mu_{brit} \tag{1}$$

$$E_{brit} = \frac{E - E_{min}}{E_{max} - E_{min}} \tag{2}$$

$$\mu_{brit} = \frac{\mu_{max} - \mu}{\mu_{max} - \mu_{min}} \tag{3}$$

In this formula, Emax, Emin, μmax, and μmin denote the maximum and minimum values of the Young′s modulus and Poisson′s ratio for the rock samples, respectively. Researchers in China analyzed the mineral composition of the Barrt shale in the Fort Worth Basin and the Lianggaoshan Formation in northeastern Sichuan. They found that the Lianggaoshan Formation has a relatively lower content of brittle minerals and a higher content of clay compared to the Barnett shale in North America, although the general distribution remains similar (Jarvie et al., 2007; Mohammad Mahdi and Reza, 2015). The brittleness index derived from this formula demonstrates a good correlation with the fracture breakdown pressure and extension pressure of shale samples in field fracturing.

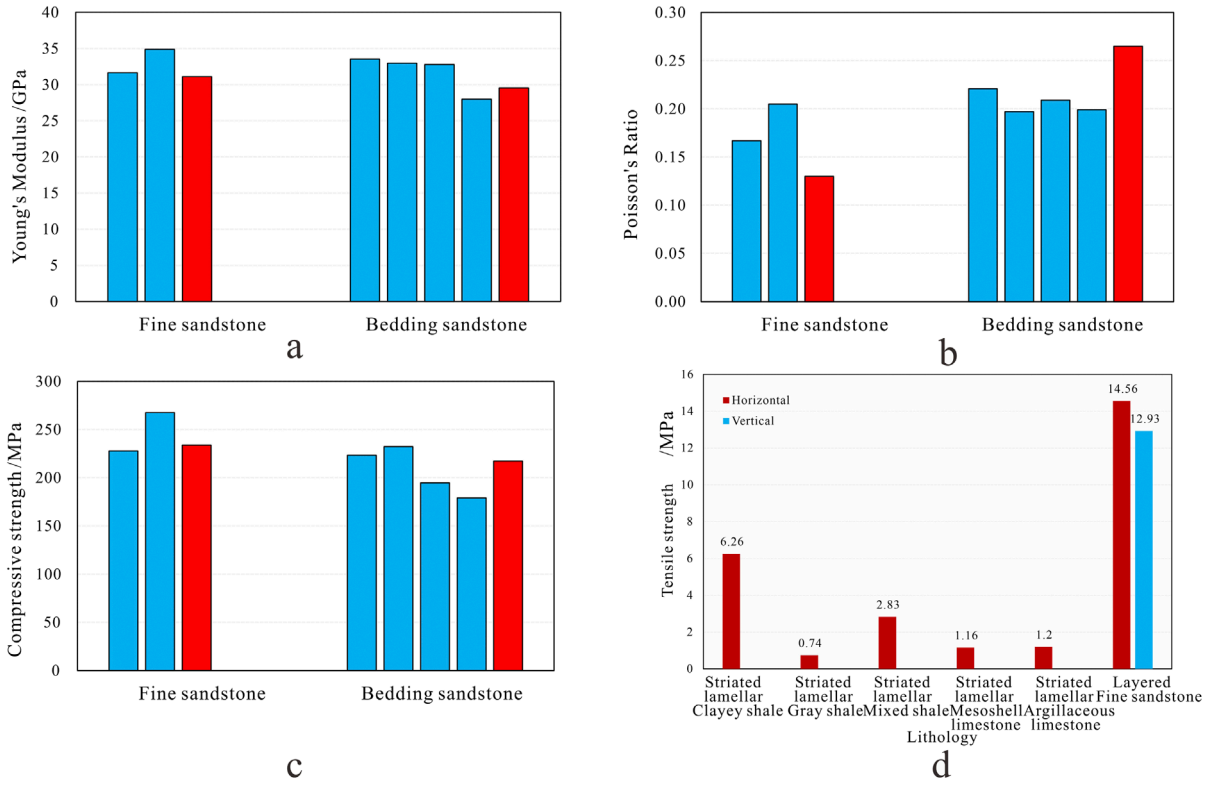

FIGURE 8
Influence of Rock Anisotropy on Rock Mechanics Parameters. **(A)** Diagram of Elastic Modulus for Different Sampling Methods of the Same Lithology in Tri-axial Experiments; **(B)** Diagram of Poisson's Ratio for Different Sampling Methods of the Same Lithology in Tri-axial Experiments; **(C)** Diagram of Compressive Strength for Different Sampling Methods of the Same Lithology in Tri-axial Experiments; **(D)** Sampling Results in Different Directions for Laminated Lithology in Tensile Experiments.

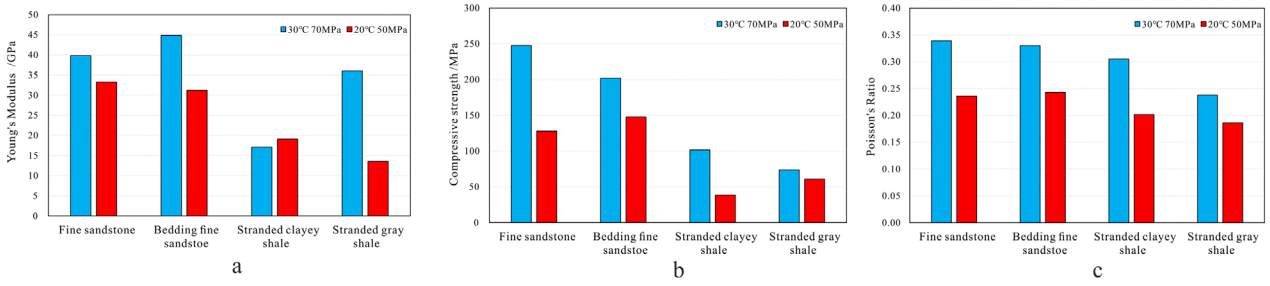

FIGURE 9
Influence of Different Temperatures and Pressures on Rock Mechanics Parameters in Tri-axial High Temperature and High Pressure Experiments. **(A)** Elastic Modulus of Samples with the Same Lithology under Different Experimental Conditions; **(B)** Poisson's Ratio of Samples with the Same Lithology under Different Experimental Conditions; **(C)** Compressive Strength of Samples with the Same Lithology under Different Experimental Conditions.

4.2 Brittleness index based on stress-strain curve

The assessment of rock brittleness features through the rock stress-strain curve has been extensively utilized in engineering applications. It reflects the complete process of rock deformation, fracture, and ultimate loss of load-bearing capacity under external loads. It enables the quantitative acquisition of rock characteristics across various stress states. This represents the most intuitive and effective approach for assessing the brittleness of rock materials. The assessment of brittleness characteristics using the stress-strain curve has gained significant application in engineering. This method mainly originates from characteristic points related to the fracture transformations of rock, such as peak stress, peak strain, residual stress, and residual strain. Formulas for assessing brittleness are developed based on the energy area or variations in characteristic

10.3389/feart.2025.1515701

TABLE 5 Calculation results of brittleness index based on the complete stress-strain curve.

Measurement number	Be1	Be2	Be3	a	b	c	BE (first)	BE (second)	BE (third)	The average brittleness value
1	201.17	0.18	25.53	0.45	0.29	0.26	0.42	0.35	0.38	0.38
2	63.17	0.27	25.63	0.41	0.37	0.22	0.23	0.33	0.30	0.29
3	133.04	0.22	12.95	0.42	0.36	0.23	0.32	0.26	0.27	0.28
4	172.01	0.35	3.92	0.48	0.07	0.45	0.21	0.22	0.22	0.22
5	207.76	0.28	19.41	0.45	0.25	0.30	0.36	0.33	0.35	0.35
6	394.78	0.14	134.31	0.45	0.32	0.23	0.89	0.91	0.91	0.90
7	89.94	0.12	11.06	0.45	0.30	0.25	0.29	0.22	0.23	0.25
8	176.42	0.18	2.20	0.37	0.26	0.37	0.30	0.28	0.28	0.29
9	100.54	0.22	0.84	0.32	0.26	0.42	0.19	0.19	0.19	0.19
10	205.71	0.16	14.64	0.42	0.27	0.31	0.40	0.35	0.35	0.36
11	321.69	0.21	36.31	0.43	0.33	0.24	0.59	0.50	0.49	0.53
12	203.56	0.21	69.60	0.41	0.31	0.28	0.50	0.60	0.58	0.56
13	192.67	0.20	17.61	0.39	0.29	0.32	0.37	0.41	0.40	0.39
14	148.73	0.27	34.05	0.39	0.34	0.27	0.34	0.34	0.30	0.33
15	197.14	0.21	29.71	0.40	0.31	0.30	0.41	0.42	0.37	0.40
16	191.42	0.23	11.15	0.36	0.28	0.35	0.33	0.37	0.36	0.35
17	143.94	0.14	4.37	0.38	0.23	0.39	0.27	0.27	0.27	0.27
18	40.56	0.29	10.73	0.39	0.36	0.24	0.17	0.20	0.18	0.18
19	75.06	0.14	3.18	0.39	0.27	0.35	0.22	0.20	0.20	0.21
20	99.86	0.41	0.36	0.31	0.34	0.35	0.13	0.12	0.12	0.13
21	179.85	0.55	0.08	0.25	0.36	0.38	0.10	0.10	0.09	0.10
22	50.47	0.33	1.62	0.36	0.36	0.28	0.14	0.15	0.14	0.14
23	69.88	0.37	0.13	0.30	0.32	0.38	0.12	0.11	0.11	0.11
24	50.23	0.37	6.48	0.37	0.38	0.25	0.13	0.13	0.12	0.13
25	112.44	0.10	4.16	0.39	0.22	0.39	0.25	0.26	0.25	0.25
26	117.55	0.48	0.00	0.33	0.40	0.26	0.12	0.12	0.12	0.12
27	217.14	0.25	4.70	0.42	0.36	0.22	0.39	0.30	0.29	0.33
28	132.39	0.36	2.68	0.31	0.33	0.36	0.19	0.19	0.19	0.19
29	271.36	−0.07	6.47	0.41	0.15	0.44	0.44	0.46	0.45	0.45
30	201.17	0.18	25.53	0.45	0.29	0.26	0.42	0.35	0.38	0.38
31	63.17	0.27	25.63	0.41	0.37	0.22	0.23	0.33	0.30	0.29
32	133.04	0.22	12.95	0.42	0.36	0.23	0.32	0.26	0.27	0.28

TABLE 6 Quantity scale.

Scale	Definition
1	In the comparison of two elements, they are regarded as having the same importance.
3	In the comparison of two elements, the former is considered to be somewhat more important than the latter.
5	In the comparison of two elements, the former is clearly more important than the latter.
7	In the comparison of two elements, the former is strongly more important than the latter.
9	In the comparison of two elements, the former is considered to be extremely more important than the latter.
2,4,6,8	Denotes the intermediate values of the previously mentioned adjacent assessments.
Reciprocal	If the importance ratio between factor i and factor j is a_{ij},then the importance ratio of factor j to factor i can be expressed as $a_{ji} = 1/a_{ij}$

TABLE 7 Judgment matrix *A*.

Significance value		A_{ij}				
		E/μ	Compression strength	Tensile strength	Cohesive strength	Angle of internal friction
A_{ij}	E/μ	1	1.5	4	5	5.5
	Compression strength	2/3	1	3	4	5
	Tensile strength	1/4	1/3	1	2	3
	Cohesive strength	1/5	1/4	2	1	2
	Angle of internal friction	2/11	1/5	1/3	1/2	1

TABLE 8 Normalized judgment matrix *A*.

Significance value	E/μ	Compression strength	Tensile strength	Cohesive strength	Angle of internal friction	ω	$A\omega$
E/μ	0.44	0.46	0.39	0.40	0.33	0.393	1.965
Compression strength	0.29	0.30	0.29	0.32	0.30	0.302	1.51
Tensile strength	0.11	0.10	0.10	0.16	0.18	0.139	0.695
Cohesive strength	0.09	0.08	0.19	0.08	0.12	0.095	0.475
Angle of internal friction	0.08	0.06	0.03	0.04	0.06	0.072	0.36

points. This study focuses on the following approaches for the evaluation of brittleness (Chen et al., 2018) (Equations 4–6):

$$B_i = B_{i1} + B_{i2} \tag{4}$$

$$B_{i1} = \frac{(\sigma_P - \sigma_i)/\delta_p}{(\varepsilon_P - \varepsilon_i)/\varepsilon_P} \tag{5}$$

$$B_{i2} = \frac{(\sigma_P - \sigma_r)/\delta_p}{(\varepsilon_r - \varepsilon_p)/\varepsilon_P} \tag{6}$$

In the equation, δ_i and δ_p are defined as the initiation stress and the peak stress, respectively. ε_i and ε_p represent the initiation strain and the peak strain. Additionally, δ_r denotes the residual stress, while ε_r signifies the residual strain. This approach considers the changes in both the pre-peak and post-peak curves, and it allows for relatively simple calculations.

The assessment of sandstone brittleness, grounded in the complete stress-strain curve and energy variations during the rock fracture process, is categorized into three main stages: work hardening and linear elastic damage, plastic deformation and

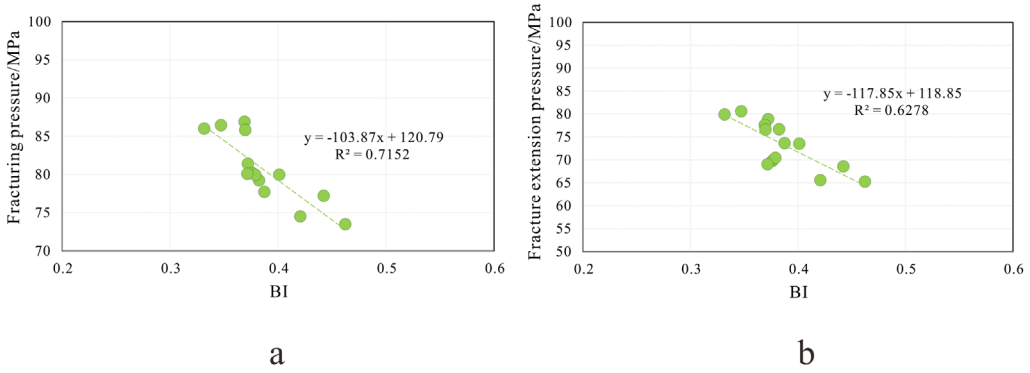

FIGURE 10
Presents the combined brittleness assessment index (BI) and its association with hydraulic fracturing. **(A)** Brittleness Index vs Breakdown Pressure; **(B)** Brittleness Index vs Fracture Extension Pressure.

damage, and failure and softening. For each sample, the stress-strain curve is analyzed, and adjustments to the theoretical programming code are made. Remapping, energy block division, and calculation of brittleness-sensitive parameters across various stages are conducted. The fuzzy analytic hierarchy process, based on energy evolution values from different stages, is used to ascertain weights and contribution values. This entire procedure is repeated three times to derive the final average (Table 5).

4.3 Construction and verification analysis of comprehensive brittleness index

The brittleness data derived from rock mechanics experiments or mineral composition tests are generally reliable, but they pose challenges such as high costs, time consumption, and the difficulty of performing comprehensive single-well profile analysis due to data dispersion. Various researchers have developed evaluation methods for shale reservoir fracturability based on logging data, which varies continuously with depth and is highly accurate. Acquiring dynamic parameters of rock mechanics from logging data is a key approach for assessing shale brittleness. Typically, dynamic rock mechanics parameters such as Young′s modulus, Poisson′s ratio, internal friction angle, and cohesion are calculated using P-wave travel time, S-wave travel time, and density logging data. The following formulas are used to calculate the dynamic rock mechanics parameters (Equations 7–12):

$$\text{Dynamic Young's Modulus:} E = \frac{\rho_b\left(3\Delta t_s^2 - 4\Delta t_p^2\right)}{\Delta t_s^2\left(\Delta t_s^2 - \Delta t_p^2\right)} \times 9.299 \times 10^7 \quad (7)$$

$$\text{Dynamic Poisson's Ratio:} \mu = \frac{\left(\Delta t_s^2 - 2\Delta t_p^2\right)}{2\left(\Delta t_s^2 - \Delta t_p^2\right)} \quad (8)$$

$$\text{Compressive Strength:} \sigma_c = \left[0.0045E\left(1 - V_{sh}\right) + 0.008EV_{sh}\right] \quad (9)$$

$$\text{Tensile Strength:} \sigma_t = \frac{\left[0.0045E\left(1 - V_{sh}\right) + 0.008EV_{sh}\right]}{12} \quad (10)$$

$$\text{Cohesion:} C = 4.69433 \times 10^7 \times \rho_b^2\left(\frac{1+\mu}{1-\mu}\right)(1-2\mu)\left(\frac{1+0.78V_{sh}}{\Delta t_p^4}\right) \quad (11)$$

$$\text{Internal Friction Angle:} \varphi = \frac{\pi}{12}\left[2\left(1 - \frac{\mu_d}{1-\mu_d}\right) + 1\right] \quad (12)$$

In this equation, ρ_b is defined as the DEN value; E denotes the dynamic Young′s modulus, expressed in GPa; μ represents the dynamic Poisson′s ratio, a dimensionless quantity; σ_c denotes the compressive strength, expressed in MPa; σ_t represents the tensile strength, quantified in MPa; C denotes the cohesion, expressed in MPa; φ represents the internal friction angle, quantified in degrees; Δt_s and Δt_p represent the travel times of shear and compressional waves, respectively, expressed in μs/m; ρ denotes the volume density of the geological formation, quantified in g/cm^3.

The brittleness index, derived from mechanical experiments, is applied to the well-logging evaluation model, five evaluation factors that significantly influence brittleness are taken into account: E/μ, compressive strength, tensile strength, cohesion, and internal friction angle (Fang et al., 2007; Lei et al., 2007a; Lei et al., 2007b). The Analytic Hierarchy Process (AHP) is employed to quantify the five parameters and conduct pairwise comparisons, thereby constructing a judgment matrix for the calculation of weights (Table 6).

A judgment matrix (A) is constructed for the factors contributing to the comprehensive brittleness indicator (BI), simultaneously, (A) is normalized by columns, followed by the calculation of the eigenvector (ω) and the product $(A\omega)$ (Tables 7, 8).

The matrix (A) is subjected to consistency evaluation, and the consistency ratio is calculated according to the following formula (Equations 13–15):

$$CR = \frac{CI}{RI} \quad (13)$$

$$CI = \frac{\lambda_{max} - n}{n-1} \quad (14)$$

$$\lambda_{max} = \sum_{i=1}^{n} \frac{[A\omega]_i}{n\omega_i} \quad (15)$$

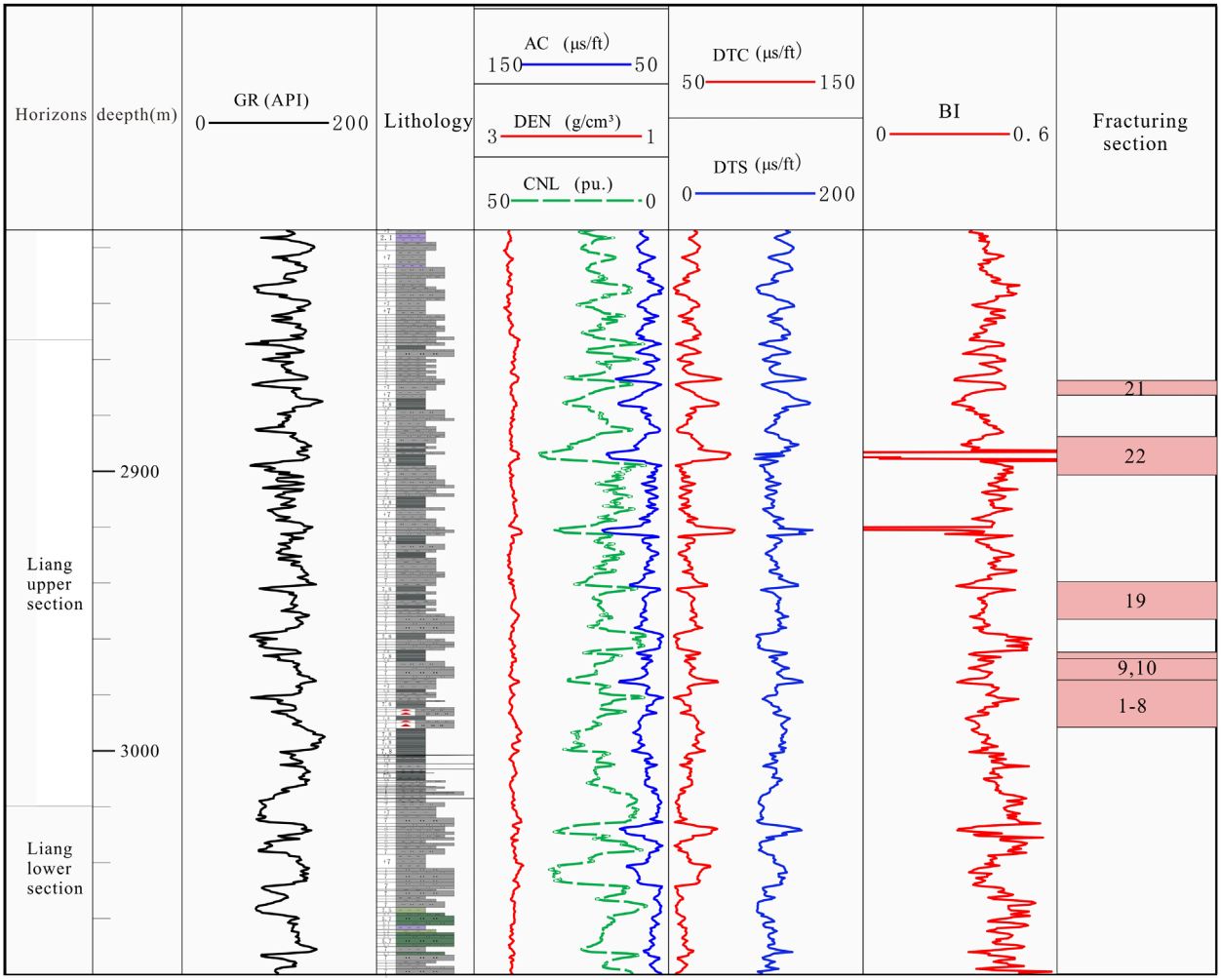

FIGURE 11
Histogram for comprehensive brittleness evaluation of well PA1.

The average random consistency index (RI) for (n = 5) is identified as 1.1075, and the calculated consistency ratio (CR = 0), which is below 0.1, signifies that the consistency has been achieved. It should be noted that the assessment of ambiguity in this study is conducted based on correlation, thereby incorporating a certain level of subjectivity. The weights assigned to (BI), compressive strength, tensile strength, cohesion, and internal friction angle in the comprehensive brittleness indicator (BI) derived from rock mechanics are determined to be 0.393, 0.302, 0.139, 0.095, and 0.072, respectively. The comprehensive brittleness evaluation metric for the Jurassic shale in northeastern Sichuan is derived as follows (Equations 16–18):

$$BI = 0.393\frac{E}{\mu} + 0.302\sigma_c + 0.139\sigma_t + 0.095C + 0.072\varphi \quad (16)$$

Ultimately, the standardization was performed using the range variation method, represented by the following formula:

$$S_p = \frac{X - X_{min}}{X_{max} - X_{min}} \quad (17)$$

$$S_n = \frac{X_{max} - X}{X_{max} - X_{min}} \quad (18)$$

In this equation, S_p and Sn indicate the standardized values of positive and negative indicators, respectively; X signifies the parameter value; X_{max} refers to the maximum parameter value; and X_{min} indicates the minimum parameter value.

The comprehensive brittleness indicator (BI), which was derived from the normalization of E/μ, compressive strength, tensile strength, cohesion, and internal friction angle, displays consistency with the fracture breakdown pressure and extension pressure observed during field fracturing. It was found that a higher brittleness index corresponds to lower fracture breakdown and extension pressures, suggesting relatively good compressibility (Figure 10). The strength of the comprehensive brittleness indicator (BI) is attributed to its consideration of a wide range of brittleness influencing factors and its solid correlation with the brittleness index obtained from the full stress-strain curve. This indicator effectively reflects the intrinsic failure characteristics of the rock and facilitates continuous evaluation in well logging, indicating that the brittleness evaluation model possesses generalizability. By applying this indicator to assess the brittleness of the PA1 upper and lower sections in the deep layers of northeastern Sichuan, it was observed

that the upper section exhibits a higher brittleness index (Figure 11), indicating a greater tendency for the shale to develop a network of fractures, which is crucial for future shale gas exploitation.

5 Conclusion

(1) The mechanical properties of Jurassic shale rocks are mainly influenced by factors such as mineral composition and confining pressure. Quartz, as a brittle mineral, affects Young′s modulus, Poisson′s ratio, and tensile strength, all of which increase with increasing quartz content. Additionally, there is a certain inverse correlation between clay content and tensile strength. After rock failure, cracks decrease with increasing confining pressure and temperature, accompanied by a significant trend of increase in Young′s modulus and Poisson′s ratio.

(2) Under triaxial experimental conditions, rock samples with well-developed bedding planes exhibit more developed cracks. In tensile experiments, shale containing laminae shows a high degree of tensile strength weakening along the laminae direction, and the more complex cracks observed after the experiment indicate that laminae, as mechanically weak planes within the rock, play an important role in rock failure.

(3) Based on the Analytic Hierarchy Process (AHP), the weights of five factors are calculated, and a comprehensive brittleness index (BI) is proposed for brittleness evaluation. This brittleness index correlates well with the fracture initiation pressure and propagation pressure during field fracturing. Overall, the Liangshang section has a higher brittleness index and is more prone to forming fracture networks, making it the primary target layer for later shale gas development.

Data availability statement

The original contributions presented in the study are included in the article/Supplementary Material, further inquiries can be directed to the corresponding authors.

Author contributions

HZ: Data curation, Writing–original draft. SY: Data curation, Methodology, Writing–original draft. XY: Data curation, Investigation, Methodology, Writing–original draft. WY: Data curation, Investigation, Methodology, Writing–original draft. GB: Writing–original draft. JZ: Writing–original draft. ZX: Data curation, Writing–original draft.

Funding

The author(s) declare that no financial support was received for the research, authorship, and/or publication of this article.

Conflict of interest

Authors HZ, SY, XY, WY, GB, and JZ were employed by Exploration and Development Research Institute of PetroChina Daqing Oilfield Co., Ltd.

The remaining author declares that the research was conducted in the absence of any commercial or financial relationships that could be construed as a potential conflict of interest.

Generative AI statement

The author(s) declare that no Generative AI was used in the creation of this manuscript.

Publisher's note

References

Altindag, R. (2010). Assessment of some brittleness indexes in rockdrilling efficiency. *Rock Mech. Rock Eng.* 43 (3), 361–370. doi:10.1007/s00603-009-0057-x

Amjad, M. R., Shakir, U., Hussain, M., Rasul, A., Mehmood, S., and Ehsan, M. (2023). Sembar Formation as an Unconventional prospect: New insights in evaluating shale gas potential combined with deep learning. *Nat. Resour. Res.* 32, 2655–2683. doi:10.1007/s11053-023-10244-x

Banerjee, R., Chakladar, S., Kumar, A., Kumar Chattopadhyay, S., and Chakravarty, S. (2024). Petrology and association of rare earth elements in magmatically altered high-ash coal of Indian origin. *Int. J. Coal Sci. Technol.* 11 (52), 52. doi:10.1007/s40789-024-00709-6

Biswas, S., Wagner, N. J., and Moroeng, O. M. (2024). Organic petrographic and mineralogical composition of the No. 6 coal seam of the Soutpansberg Coalfield, South Africa: Insights into paleovegetation and depositional environment. *Int. J. Coal Sci. Technol.* 11 (41), 41. doi:10.1007/s40789-024-00698-6

Cai, M., Liu, D., and He, M. (2002). *Rock mechanics and engineering[M]*. Beijing: Science Press, 70–71.

Cao, F., He, J., Cao, H., Deng, H., Jiang, R., Wang, W., et al. (2024d). Multi-scale rock mechanical parameters and quantitative assessment of brittleness in alkaline lacustrine shale reservoirs. *J. Chengdu Univ. Technol. Nat. Sci. Ed.*, 1–23.

Cao, Z., Yang, X., Zhang, P., and Feng, D. (2024c). Evolution mechanism of water-conducting fractures in overburden under the influence of water-rich fault in underground coal mining. *Sci. Rep.* 14, 5081. doi:10.1038/s41598-024-54803-5

Cao, Z., Yang, X., Zhang, P., Zhenhua, L., Feng, D., Wenqiang, W., et al. (2024a). Experimental study on the fracture surface morphological characteristics and permeability characteristics of sandstones with different particle sizes. *Energy Sci. & Eng.* 12 (7), 2798–2809. doi:10.1002/ese3.1768

Cao, Z., Yang, X., Zhenhua, Li, Cunhan, H., Feng, D., Wenqiang, W., et al. (2024b). Fracture propagation and pore pressure evolution characteristics induced by hydraulic and pneumatic fracturing of coal. *Sci. Rep.* 14, 9992. doi:10.1038/s41598-024-60873-2

Chakladar, S., Kumari, S., Kumar, A., Mohanty, A., Chakravarty, S., and Kolker, A. (2024). Distribution of trace elements and rare earth elements in coal from the

Bhalukasba Surni coal block, Rajmahal coalfield, Eastern India. *Int. J. Coal Sci. Technol.* 11 (81), 81. doi:10.1007/s40789-024-00729-2

Chen, G., Cong, Z., Tao, W., and Wang, J. (2018). Evaluation method of rock brittleness characteristics based on full stress-strain curve and initiation stress. *Chin. J. Rock Mech. Eng.* 37 (1), 52–58. doi:10.13722/j.cnki.jrme.2017.0499

Du, J., Hu, S., Pang, Z., Lin, S., Hou, L., and Zhu, R. (2009). The types, potentials and prospects of continental shale oil in China. *China Pet. Explor.* 24 (5), 560–568. doi:10.3969/j.issn.1672-7703.2019.05.003

Ehsan, M., Chen, R., Latif, M. A. U., Abdelrahman, K., Ali, A., Ullah, J., et al. (2024a). Unconventional reservoir characterization of patala formation, upper Indus basin, Pakistan. *ACS Omega* 9 (13), 15573–15589. doi:10.1021/acsomega.4c00465

Ehsan, M., Zaheer, A. M., and Abbasi, M.Ul H. (2024b). Estimating total organic carbon (TOC) content and porosity of the Ranikot Formation in the central Indus basin, Pakistan, using seismic inversion and well log analysis. *J. GeoEnergy* 2024, 1–12. doi:10.1155/2024/5568380

Fang, L., Chen, Y., Jun, Y., Sun, X., and Lei, Z. (2007). Application of fuzzy analytic hierarchy process based on variable weight in profile control well selection in low permeability reservoirs. *Special Oil & Gas Reservoirs* (03), 81–84. doi:10.3969/j.issn.1006-6535.2007.03.023

Fu, Y., Ma, F., and Zeng, L. (2011). Key techniques for fracturing experimental evaluation of shale gas reservoirs. *Nat. Gas. Ind.* 31 (4), 51–54. doi:10.3787/j.issn.1000-0976.2011.04.012

Guo, X., Yongqiang, Z., Shen, B., Wei, X., Lu, L., Pan, A., et al. (2022). Marineshale gas exploration theory in southern China: review and prospects. *Acta Geol. Sin.* 96 (1), 172–182. doi:10.19762/j.cnki.dizhixuebao.2022271

He, W., He, H., Wang, Y., Cui, B., Meng, Q., Guo, X., et al. (2022). Major breakthrough and significance of shale oil of the Jurassic Lianggaoshan Formation in well Pingan 1 in northeastern Sichuan Basin. *China Pet. Explor.* 27 (1), 40–49. doi:10.3969/j.issn.1672-7703.2022.01.004

Jarvie, D. M., Hill, R., Ruble, T., and Pollastro, R. M. (2007). Unconventional shale-gas systems: the Mississippian Barnett Shale of north-central Texas as one model for thermogenic shale-gas assessment. *Bulletin* 91 (4), 475–499. doi:10.1306/12190606068

Jiang, Y., Dong, D., and Qi, L. (2010). Basic characteristics and evaluation of shale gas reservoirs. *Nat. Gas. Ind.* 30 (10), 7–12. doi:10.3787/j.issn.1000-0976.2010.10.002

Jin, Z., Wang, G., Liu, G., Gao, Bo, Liu, Q., Wang, H., et al. (2021). Research progress and key scientific issues of continental shale oil in China. *Acta Pet. Sin.* 42 (7), 821–835. doi:10.7623/syxb202107001

Li, Q., Chen, M., Wang, F. P., Jin, Y., and Li, Z. (2012a). The influence of engineering factors on shale gas production: Taking the Haynesville shale gas reservoir in North America as an example. *Nat. Gas. Ind.* 32(4), 54–59. doi:10.3787/j.issn.1000-0976.2012.04.013

Li, Q., Chen, M., Jin, J., Hou, B., and Zhang, J. (2012b). Indoor evaluation method and improvement of shale brittleness. *Chin. J. Rock Mech. Eng.* 31(08), 1680–1685. doi:10.3969/j.issn.1001-0890.2012.04.004

Li, Q., Chen, M., Jin, Y., Zhao, F., and Jiang, H. (2012c). Rock mechanical properties and brittleness evaluation of shale gas reservoirs. *Pet. Drill. Technol.* 40(04), 17–22. doi:10.3969/j.issn.1006-6535.2013.01.040

Li, J. (2013). Mineral composition and brittleness analysis of shale in Dongying Sag. *Acta Sedimentol. Sin.* 31 (04), 616–620. doi:10.14027/j.cnki.cjxb.2013.04.008

Lei, Z., Chen, Y., and Yaodong, Xu (2007a). Comprehensive evaluation of reservoir profile control suitability using fuzzy analytic hierarchy process. *Daqing Petroleum Geol. Dev.* (03), 82–86. doi:10.3969/j.issn.1000-3754.2007.03.019

Lei, Z., Chen, Y., and Yaodong, Xu (2007b). Comprehensive evaluation of reservoir profile control suitability using fuzzy analytic hierarchy process. *Daqing Petroleum Geol. Dev.* (03), 82–86. doi:10.3969/j.issn.1000-3754.2007.03.019

Li, Y., He, J., Deng, H., Wei, L., Wang, Y., Li, R., et al. (2024). The present-day *in-situ* stress filed characyeristic of deep shale reservoirs: a case study og Yongchuan shale gas filed in South Sichuan Basin. *J. China Univ. Min. & Technol.* 53 (3), 546–563. doi:10.13247/j.cnki.jcumt.20230307

Mohammad Mahdi, L., and Reza, R. (2015). The importance of geochemical parameters and shale composition on rock mechanical properties of gas shale reservoirs: a case study from the Kockatea shale and Carynginia formation from the Perth basin, Western Australia. *Rock Mech. Rock Eng.* 48 (3), 1249–1257. doi:10.1007/s00603-014-0617-6

Nelson, R. A. (2001). Geologic analysis of naturally fractured reservoirs. *Geol. Analysis Nat.* (4), 323–332.

Qiao, W., Hu, Li, and Ting, L. (2020). Characterization methods and main controlling factors of shale brittleness. *Fault Block Oil Gas Field* 27 (04), 458–463.

Rahimzadeh, K. I., Ameri, M., and Molladavoodi, H. (2018). Shale brittleness evaluation based on energy balance analysis of stress-strain curves. *J. Petroleum Sci. Eng.* 167, 1–19. doi:10.1016/j.petrol.2018.03.061

Reedy, R. C., Scanlon, B. R., Bagdonas, D. A., Hower, J. C., James, D., Richard Kyle, J., et al. (2024). Coal ash resources and potential for rare earth element production in the United States. *Int. J. Coal Sci. Technol.* 11 (74), 74. doi:10.1007/s40789-024-00710-z

Rickman, R., Mullen, M. J., and Petre, E. J. (2008). *A practical use of shale petrophysics for stimulation design optimization:All shale plays are not clones of the Barnett Shale[R]*. Colorado,USA. doi:10.2118/115258-ms

Saberi, F., and Hosseini-Barzi, M. (2024). Effect of thermal maturation and organic matter content on oil shale fracturing. *Int. J. Coal Sci. Technol.* 11 (16), 16. doi:10.1007/s40789-024-00666-0

Sang, S., Zheng, S., Wang, J., Zhou, X., Liu, X., Han, S., et al. (2023). Application of new rock mechanical stratigraphy in sweet spot prediction for deep coalbed methaneexploration and development. *Acta Pet. Sin.* 44 (11), 1840–1853. doi:10.7623/syxb202311007

Xiong, J., Wu, J., Liu, X., Li, B., Zhang, J., and Liang, L. (2024). Study on rock mechanical properties of different lithologies in marine continental transitional formation: a case study of the Shanxi Formation in the eastern margin of Ordos Basin. *Prog. Geophys.* 39 (2), 759–769. doi:10.6038/pg2024HH0165

Xuefeng, B., Wang, M., Xin, W., Junhui, Li, Shuangfang, Lu, Xinyi, Y., et al. (2024). Evaluation of sweet spots and enrichment areas of shale oil in the Jurassic Lianggaoshan Formation in northeastern Sichuan Basin [J/OL]. *Earth Sci.*, 1–27. doi:10.3799/dqkx.2024.075

Yang, L., and Jin, Z. (2019). Global shale oil development and prospects. *China Pet. Explor.* 24(5), 553–559. doi:10.3969/j.issn.1672-7703.2019.05.002

Yuan, J., Deng, J., Zhang, D., Li, D., Yan, W., Chen, C., et al. (2021). Fracturing evaluation technology for shale gas reservoirs. *Acta Pet. Sin.* 34 (03), 523–527. doi:10.7623/syxb201303015

Wang, Y., Deng, H., He, J., Xie, J., Hou, L., and Xu, Q. (2021). Rock fracture toughness of the second member of Xujiahe Member in Hechuan area, Chongqing. *J. Chengdu Univ. Technol. Nat. Sci. Ed.* 48 (02), 178–185. doi:10.3969/j.issn.1671-9727.2021.02.05

Zhang, J., Ai, C., Li, Y., Zeng, J., and Qiu, D. (2017). Brittleness evaluation index based on energy evolution in the whole process of rock failure. *Chin. J. Rock Mech. Eng.* 36 (06), 1326–1340. doi:10.13722/j.cnki.jrme.2016.0839

Zhang, C., Wang, Y., Dong, D., and Guan, Q. (2016). The brittleness characteristics of shale from Wufeng formation to Longmaxi Formation in Changning area, southern Sichuan. *Nat. Gas. Geosci.* 27 (09), 1629–1639. doi:10.11764/j.issn.1672-1926.2016.09.1629

Zhang, Y., Fan, C., Zhong, C., Ye, Z., Qin, Q., and Li, R. (2018). Research on brittleness evaluation method of organic-rich shale in complex geological features. *Geol. Prospect.* 54 (05), 1069–1083. doi:10.3969/j.issn.0495-5331.2018.05.018

Zhao, Y., Sun, Z., and Liu, B. (2019). Comparative study on semicircular bending test of type I and type II fracture characteristics of Xinzhouyao bituminous coal. *Chin. J. Rock Mech. Eng.* 38 (8), 1594–1603. doi:10.13722/j.cnki.jrme.2019.0306

Zheng, Y. (1988). *Mine rock Mass mechanics[M]*. Beijing: Metallurgical Industry Press, 9–10.

Zhong, C., Qin, Q., Zhou, J., Hu, D., and Wei, Z. (2018). Evaluation of brittleness of organic-rich shale of Longmaxi Formation in Dingshan area, southeastern Sichuan. *Geol. Sci. Technol. Inf.* 37 (04), 167–174. doi:10.19509/j.cnki.dzkq.2018.0422

Ziba, Z., Hossain, R.-B., and Ralf, L. (2023). Coal petrology, sedimentology and depositional environment of the Parvadeh coals in the upper Triassic, Tabas block of central-East Iran. *Int. J. Coal Sci. Technol.* 10 (1), 40. doi:10.1007/s40789-023-00600-w